

Multiple scattering in discrete random media using first-order incoherent interactions

K. Muinonen^{1,2*}, J. Markkanen¹, T. Väisänen¹, J. I. Peltoniemi², and A. Penttilä¹

¹Department of Physics, University of Helsinki, P.O. Box 64, Gustaf Hällströmin katu 2a, FI-00014 University of Helsinki, Finland

²Finnish Geospatial Research Institute FGI, National Land Survey of Finland, Geodeetinrinne 2, FI-02430 Masala, Finland

Key Points:

- We introduce incoherent extinction, scattering, and absorption into the radiative-transfer coherent-backscattering method (RT-CB).
- Consequently, we extend the applicability of the RT-CB from sparse to dense discrete random media.
- The results compare favorably to those from the asymptotically exact Superposition T -matrix method.

*Department of Physics, University of Helsinki, Gustaf Hällströmin katu 2a, P.O. Box 64, FI-00014 U. Helsinki, Finland

Corresponding author: Karri Muinonen, karri.muinonen@helsinki.fi

Abstract

We consider scattering of electromagnetic waves by a finite discrete random medium composed of spherical particles. The size of the random medium can range from microscopic sizes of a few wavelengths to macroscopic sizes approaching infinity. The size of the particles is assumed to be of the order of the wavelength. We extend the numerical Monte Carlo method of radiative transfer and coherent backscattering (RT-CB) to the case of dense packing of particles. We adopt the ensemble-averaged first-order incoherent extinction, scattering, and absorption characteristics of a volume element of particles as input for the RT-CB. The volume element must be larger than the wavelength but smaller than the mean free path length of incoherent extinction. In the radiative transfer part, at each absorption and scattering process, we account for absorption with the help of the single-scattering albedo and peel off the Stokes parameters of radiation emerging from the medium in predefined scattering angles. We then generate a new scattering direction using the joint probability density for the local polar and azimuthal scattering angles. In the coherent backscattering part, we utilize amplitude scattering matrices along the radiative-transfer path and the reciprocal path, and utilize the reciprocity of electromagnetic waves to verify the computation. We illustrate the incoherent volume-element scattering characteristics and compare the dense-medium RT-CB to asymptotically exact results computed using the Superposition T -matrix method (STMM). We show that the dense-medium RT-CB compares favorably to **the STMM** for the current cases of sparse and dense discrete random media studied.

1 Introduction

Multiple electromagnetic scattering in discrete random media of particles constitutes a challenging computational problem in classical electromagnetics. Whereas wavelength-scale random media can be assessed accurately using, for example, the Superposition T -Matrix (STMM; e.g., [1; 2] and Volume-Integral-Equation Methods (VIEM; e.g., [3]), unsurmountable computational difficulties arise for random media much larger than the wavelength. Furthermore, whereas the classical radiative transfer approximation accompanied with coherent backscattering (**RT-CB**; [4]) has been validated for sparse random media with particle volume densities smaller than $\sim 5\%$ [5], no accurate computational methods are available for dense random media with high volume densities.

Our scientific motivation for resolving the open computational problem derives from two ubiquitous astrophysical phenomena observed at small solar phase angles (the Sun-Object-Observer angle) for the Moon, asteroids, Saturn's rings, transneptunian objects, and atmosphereless Solar System objects at large. First, a nonlinear increase of brightness, commonly called *the opposition effect* (e.g., [6]), is observed toward the zero phase angle in the magnitude scale. Second, the scattered light is observed to be partially linearly polarized parallel to the Sun-Object-Observer plane, commonly called *negative polarization* ([7]). **This is contrary to the common positive polarization perpendicular to the scattering plane arising from Rayleigh scattering and Fresnel reflection.** In 1980s, the coherent-backscattering mechanism was suggested as a partial explanation for the phenomena [8; 9].

The RT-CB Monte Carlo ray-tracing method relies on exponential extinction in a homogeneous scattering and absorbing medium, where the scatterers are assumed to be in each others' far-field regimes. Multiple scattering takes place in the far-field approximation and is fully described by the 2×2 Jones scattering amplitude matrices for the incident, fully transversely polarized electromagnetic field. The field representation is required due to the tracing of the electromagnetic phase difference between wave components interacting along reciprocal paths. The 4×4 Mueller scattering matrices are

utilized, for example, in the generation of new interaction directions and in the numerical integration of the radiative-transfer-only signal (RT-only).

We generalize the RT-CB for dense discrete random media of scattering and absorbing particles **by introducing** incoherent first-order interactions among volume elements of particles within the random media (for an early approach, see [10; 11]). **In the first-order approximation, the scattered field of a given volume-element realization is the sum of the fields due to the individual spherical particles, accounting for the electromagnetic phase of the incident field as well as the phase originally due to the Green's function.** In size, the volume elements must be of the order of the wavelength or larger, but nevertheless smaller than the extinction mean free path of the medium. **The discrete random medium is considered to be fully packed with the volume elements, that is, the volume density of the elements is 100%.**

Our approach has been triggered, first, **by the earlier Monte Carlo studies on volume-element extinction in random media of particles with sizes near and within the Rayleigh regime [12; 13].** Second, earlier studies mostly based on the Percus-Yevick approximation (e.g., [14; 15]) as well as the more recent derivation of the RT equation from the Maxwell equations for sparse discrete random media [16] **have encouraged us to search for more precise RT-related multiple scattering methods for dense media.** In summary, introducing incoherent volume elements promises to remove shortcomings in classical RT for sparse random media.

In Sect. 2, we present the basic theoretical framework for scattering and absorption by spherical particles. We then describe multiple scattering in discrete spherical random media with sizes varying from the length scale of a few wavelengths upwards. We introduce the incoherent extinction, scattering, and absorption coefficients of a volume element of particles. Section 3 provides an assessment of the numerical methods for the computation of the extinction, scattering, and absorption coefficients, as well as the incoherent scattering matrix elements. We also describe the key points of the Monte Carlo RT-CB method. In Sect. 4, we show our first results for incoherent volume-element scattering characteristics and compare the results to those obtained using the STMM. In Sect. 5, we close the work with conclusions and future prospects.

2 Scattering theory

2.1 Spherical particles

Consider incident electromagnetic plane wave field in free space with wavelength λ and wave number $k = 2\pi/\lambda$. For a spherical particle with size parameter $x = ka$ (a is radius) and complex refractive index m isolated in free space, the extinction, scattering, and absorption cross sections (**respectively** σ_e , σ_s , and σ_a) and efficiencies (q_e , q_s , and q_a) are [17]

$$\begin{aligned} q_e &= \frac{\sigma_e}{\pi a^2} = \frac{2}{x^2} \sum_{l=1}^{\infty} (2l+1) \text{Re}(a_l + b_l), \\ q_s &= \frac{\sigma_s}{\pi a^2} = \frac{2}{x^2} \sum_{l=1}^{\infty} (2l+1) (|a_l|^2 + |b_l|^2), \\ q_a &= \frac{\sigma_a}{\pi a^2} = q_e - q_s. \end{aligned} \quad (1)$$

Here a_l and b_l are the vector spherical harmonics coefficients of the scattered electromagnetic field:

$$\begin{aligned} a_l &= \frac{m\psi_l(mx)\psi_l'(x) - \psi_l(x)\psi_l'(mx)}{m\psi_l(mx)\xi_l'(x) - \xi_l(x)\psi_l'(mx)}, \\ b_l &= \frac{\psi_l(mx)\psi_l'(x) - m\psi_l(x)\psi_l'(mx)}{\psi_l(mx)\xi_l'(x) - m\xi_l(x)\psi_l'(mx)}. \end{aligned} \quad (2)$$

105 where ψ_l and ξ_l are Riccati-Bessel functions and strictly related to the spherical Bessel
 106 and Hankel functions j_l and $h_l^{(1)}$,

$$\begin{aligned}\psi_l(x) &= x j_l(x), \\ \xi_l(x) &= x h_l^{(1)}(x).\end{aligned}\quad (3)$$

107 The single-scattering albedo is

$$\tilde{\omega} = \frac{q_s}{q_e} = \frac{\sigma_s}{\sigma_e}.\quad (4)$$

108 The scattering matrix \mathbf{S} and the normalized scattering phase matrix \mathbf{P} for spher-
 109 ical particles are (superscript LM for Lorenz-Mie)

$$\begin{aligned}\mathbf{S}^{\text{LM}} &= \frac{k^2 \sigma_s}{4\pi} \mathbf{P}^{\text{LM}}, \\ \mathbf{P}^{\text{LM}} &= \frac{2}{x^2 q_s} \begin{pmatrix} |S_{\parallel\parallel}|^2 + |S_{\perp\perp}|^2 & |S_{\parallel\parallel}|^2 - |S_{\perp\perp}|^2 & 0 & 0 \\ |S_{\parallel\parallel}|^2 - |S_{\perp\perp}|^2 & |S_{\parallel\parallel}|^2 + |S_{\perp\perp}|^2 & 0 & 0 \\ 0 & 0 & \text{Re}(S_{\perp\perp}^* S_{\parallel\parallel}) & \text{Im}(S_{\perp\perp}^* S_{\parallel\parallel}) \\ 0 & 0 & -\text{Im}(S_{\perp\perp}^* S_{\parallel\parallel}) & \text{Re}(S_{\perp\perp}^* S_{\parallel\parallel}) \end{pmatrix}, \\ &\int_{4\pi} \frac{d\Omega}{4\pi} P_{11}^{\text{LM}}(\Omega) = 1,\end{aligned}\quad (5)$$

110 where the amplitude scattering matrix elements $S_{\perp\perp}$ and $S_{\parallel\parallel}$ are

$$\begin{aligned}S_{\perp\perp} &= \sum_{l=1}^{\infty} \frac{2l+1}{l(l+1)} \left[a_l \frac{dP_l^1(\cos\theta)}{d\theta} + b_l \frac{1}{\sin\theta} P_l^1(\cos\theta) \right], \\ S_{\parallel\parallel} &= \sum_{l=1}^{\infty} \frac{2l+1}{l(l+1)} \left[a_l \frac{1}{\sin\theta} P_l^1(\cos\theta) + b_l \frac{dP_l^1(\cos\theta)}{d\theta} \right],\end{aligned}\quad (6)$$

111 and P_l^1 are associated Legendre functions.

117 2.2 Superposition T -matrix method

118 Consider electromagnetic scattering by a system of multiple non-intersecting spheres
 119 in the frequency domain using the Maxwell equations. The scattering problem can be
 120 solved by applying the superposition principle, i.e., the total scattered field \mathbf{E}^s can be
 121 represented as a sum of partially scattered fields \mathbf{E}_i^s from each sphere:

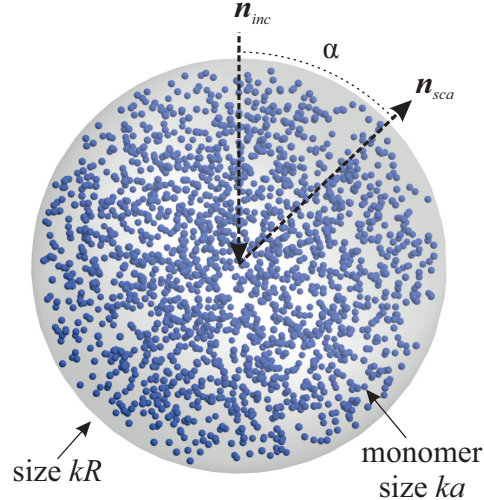
$$\mathbf{E}^s = \sum_{i=1}^N \mathbf{E}_i^s,\quad (7)$$

122 in which N is the number of spheres. The partial fields are expanded with the spheri-
 123 cal vector wave functions \mathbf{M}_ν expressed with respect to the origin of the i th sphere as

$$\mathbf{E}_i^s \approx \sum_{\nu} a_i^{\nu} \mathbf{M}_\nu,\quad (8)$$

124 where a_i are the scattering coefficients and ν is the multi-index $\nu = \{n, m, k\}$ with $n =$
 125 $1, \dots, N$, $m = -n, \dots, n$, and $k = 1, 2$. The scattering equations in coefficient space
 126 can be expressed as

$$a_i^{\text{sca}} = T_i a_i^{\text{inc}} + T_i \sum_{j=1, j \neq i}^N (S|R)_i^j a_j^{\text{sca}} \quad \text{for all } i = 1, \dots, N\quad (9)$$



112 **Figure 1.** Discrete spherical random medium of equal-sized spherical particles. The phase
 113 angle α denotes the angle between the source of illumination (in the direction $-\mathbf{n}_{inc}$) and the
 114 observer (\mathbf{n}_{sca}) as seen from the object. The scattering angle is $\theta = \pi - \alpha$. The size parameters
 115 of the random medium and of the particles are kR and ka , respectively. Finally, $k = 2\pi/\lambda$ is
 116 **the wave number and** λ is the wavelength.

127 where T_i is the T -matrix of the i th sphere and $(S|R)_i^j$ is the translation matrix that trans-
 128 lates the coefficients a_j^{sca} **of the scattered field by sphere j** into the incoming coef-
 129 ficients of sphere i [18].

130 The scattering equations (9) are solved iteratively by the Generalized Minimum
 131 Residual method (GMRES). The matrix-vector multiplication, required in each itera-
 132 tion step, is accelerated by the Fast Multipole Method (FMM) [19; 20]. In our imple-
 133 mentation (FaSTMM, [2]), the so-called rotation \rightarrow axial translation \rightarrow inverse rotation
 134 technique is used with recursive computations of the axial translation [21] and rotation
 135 coefficients [22].

136 2.3 Scattering by discrete random media

137 Consider next a finite, spherical medium (radius R , size parameter $X = kR$) of
 138 randomly distributed spherical particles with a volume density of v (Fig. 1). The finite
 139 medium is assumed to be located in free space and an RT-CB solution is searched for
 140 the extinction, scattering, and absorption characteristics of the medium. It is here pos-
 141 tulated that the incoherent extinction, scattering, and absorption characteristics for a
 142 volume element of the medium are needed as input for the numerical method.

143 In order to proceed, we utilize the spherical geometry once more: consider a spheri-
 144 cal volume element (radius R_0 , **size parameter** $X_0 = kR_0$) completely within the ran-
 145 dom medium. We assign a spherical particle to the volume element if the particle center
 146 is located within the element. We envisage that the volume density is approximately
 147 balanced by the omission of particles intersecting the volume element but with their cen-
 148 ters nevertheless outside the volume element. Furthermore, for the time being, we omit
 149 any surface effects arising from the volume element intersecting the boundary of the ran-
 150 dom medium.

151 Due to the stochastic nature of the random medium, the number and location of
 152 the spherical particles within the volume element will vary both as a function of the el-

153 element location in the random-medium realization and from one random-medium realization to another.
154

155 **Let us derive the ensemble-averaged incoherent extinction, scattering,**
156 **and absorption coefficients of the volume element. We write the ensemble-**
157 **averaged first moment of the field scattered by the volume element (the mean**
158 **or coherent scattered field) as**

$$\mathbf{E}^{\text{s},c}(\mathbf{r}) = \langle \mathbf{E}^{\text{s}}(\mathbf{r}) \rangle = \lim_{n \rightarrow \infty} \frac{1}{n} \sum_{i=1}^n \mathbf{E}_i^{\text{s}}(\mathbf{r}), \quad (10)$$

159 where n is the number of volume-element realizations, and \mathbf{E}_i^{s} is the scattered field from
160 volume-element realization i .

161 The incoherent scattered field from volume-element realization i is then obtained
162 by subtracting the coherent scattered field from the scattered field of the realization,

$$\mathbf{E}_i^{\text{s},ic}(\mathbf{r}) = \mathbf{E}_i^{\text{s}}(\mathbf{r}) - \mathbf{E}^{\text{s},c}(\mathbf{r}). \quad (11)$$

163 Consequently, the first moment of the incoherent scattered field vanishes,

$$\langle \mathbf{E}^{\text{s},ic}(\mathbf{r}) \rangle \equiv 0, \quad (12)$$

164 and the second moment of the incoherent scattered field equals

$$\langle |\mathbf{E}^{\text{s},ic}(\mathbf{r})|^2 \rangle = \langle |\mathbf{E}^{\text{s}}(\mathbf{r})|^2 \rangle - |\mathbf{E}^{\text{s},c}(\mathbf{r})|^2. \quad (13)$$

165 **Within the present framework, the second moment of the scattered field thus**
166 **equals the sum of the second moment of the incoherent field and the abso-**
167 **lute value of the coherent field squared.**

168 In the first-order approximation, the scattered far field of volume-element realiza-
169 tion i at distance r is the sum of the free-space scattered fields of the N_i identical spher-
170 ical particles with scattering amplitude \mathbf{A}^{s} located at \mathbf{r}_j ($j = 1, \dots, N_i$):

$$\begin{aligned} \mathbf{E}_i^{\text{s}}(\mathbf{r}) &= \sum_{j=1}^{N_i} \mathbf{E}_{ij}^{\text{s}}(\mathbf{r}_j) = \frac{\exp(ikr)}{-ikr} \mathbf{A}^{\text{s}} \sum_{j=1}^{N_i} \exp(i\mathbf{q} \cdot \mathbf{r}_j), \\ \mathbf{q} &= \mathbf{k}^{\text{i}} - \mathbf{k}^{\text{s}}, \end{aligned} \quad (14)$$

171 where $\mathbf{k}^{\text{i}} = k\mathbf{e}_z$ and \mathbf{k}^{s} denote the wave vectors of the incident and scattered fields, re-
172 spectively.

173 The coherent scattered far field is thus the ensemble average

$$\mathbf{E}^{\text{s},c}(\mathbf{r}) = \frac{\exp(ikr)}{-ikr} \mathbf{A}^{\text{s}} \lim_{n \rightarrow \infty} \frac{1}{n} \sum_{i=1}^n \sum_{j=1}^{N_i} \exp(i\mathbf{q} \cdot \mathbf{r}_j^{(i)}), \quad (15)$$

174 where $\mathbf{r}_j^{(i)}$ denotes the location of particle j for the realization i . The incoherent far field
175 of a single realization follows from Eqs. 11, 14, and 15.

176 We can improve the convergence of ensemble-averaging with the help of analyti-
177 cal averaging over orientations. For the coherent scattered field, instead of averaging as
178 in Eq. 15, we average as follows:

$$\begin{aligned} \mathbf{E}^{\text{s},c}(\mathbf{r}) &= \frac{\exp(ikr)}{-ikr} \mathbf{A}^{\text{s}} \lim_{n \rightarrow \infty} \frac{1}{n} \sum_{i=1}^n \sum_{j=1}^{N_i} \frac{\sin qr_j^{(i)}}{qr_j^{(i)}}, \\ q &= |\mathbf{q}| = 2k \sin \frac{1}{2} \theta. \end{aligned} \quad (16)$$

179 Similarly, for the squared scattered far field, we obtain ([23], see also the Rayleigh-Gans
180 treatment in [24])

$$|\mathbf{E}^s(\mathbf{r})|^2 = \frac{1}{k^2 r^2} |\mathbf{A}^s|^2 \lim_{n \rightarrow \infty} \frac{1}{n} \sum_{i=1}^n \sum_{j=1}^{N_i} \sum_{k=1}^{N_i} \frac{\sin q |\mathbf{r}_j^{(i)} - \mathbf{r}_k^{(i)}|}{q |\mathbf{r}_j^{(i)} - \mathbf{r}_k^{(i)}|}. \quad (17)$$

181 It now follows that the ensemble-averaged incoherent scattering matrix of the vol-
182 ume element is a pure Mueller matrix obtained by multiplying the Mie scattering ma-
183 trix in Eq. 5 by a function $H(\theta)$,

$$\begin{aligned} \mathbf{S}_0^{\text{ic}}(\theta) &= H(\theta) \mathbf{S}^{\text{LM}}(\theta), \\ H(\theta) &= F(\theta) - G(\theta), \\ F(\theta) &= \lim_{n \rightarrow \infty} \frac{1}{n} \sum_{i=1}^n \sum_{j=1}^{N_i} \sum_{k=1}^{N_i} \frac{\sin q |\mathbf{r}_j^{(i)} - \mathbf{r}_k^{(i)}|}{q |\mathbf{r}_j^{(i)} - \mathbf{r}_k^{(i)}|}, \\ G(\theta) &= \left| \lim_{n \rightarrow \infty} \frac{1}{n} \sum_{i=1}^n \sum_{j=1}^{N_i} \frac{\sin q r_j^{(i)}}{q r_j^{(i)}} \right|^2, \end{aligned} \quad (18)$$

184 where $F(\theta)$ is the well-known form factor. Furthermore, we can assign a diagonal inco-
185 herent amplitude scattering matrix for the volume element,

$$\begin{aligned} S_{\perp\perp,0}^{\text{ic}}(\theta) &= \sqrt{H(\theta)} S_{\perp\perp}(\theta), \\ S_{\parallel\parallel,0}^{\text{ic}}(\theta) &= \sqrt{H(\theta)} S_{\parallel\parallel}(\theta). \end{aligned} \quad (19)$$

186 The ensemble-averaged incoherent scattering cross section of the volume element
187 **results from**

$$\sigma_{s,0}^{\text{ic}} = \frac{1}{k^2 r^2} \int_{4\pi} d\Omega S_{0,11}^{\text{ic}}(\theta), \quad (20)$$

188 and, consequently, the incoherent scattering coefficient is

$$\kappa_s^{\text{ic}} = \frac{\sigma_{s,0}^{\text{ic}}}{V_0}, \quad V_0 = \frac{4\pi}{3} R_0^3. \quad (21)$$

189 The incoherent absorption cross section of the volume element as well as the incoher-
190 ent absorption coefficient scale with the help of the **incoherent scattering cross sec-
191 tion and the cross sections of the spherical particle**,

$$\sigma_{a,0}^{\text{ic}} = \frac{\sigma_{s,0}^{\text{ic}}}{\sigma_s} \sigma_a, \quad \kappa_a^{\text{ic}} = \frac{\sigma_{a,0}^{\text{ic}}}{V_0}. \quad (22)$$

192 The incoherent extinction **cross section and coefficient are**

$$\sigma_{e,0}^{\text{ic}} = \sigma_{s,0}^{\text{ic}} + \sigma_{a,0}^{\text{ic}}, \quad \kappa_e^{\text{ic}} = \frac{\sigma_{e,0}^{\text{ic}}}{V_0}. \quad (23)$$

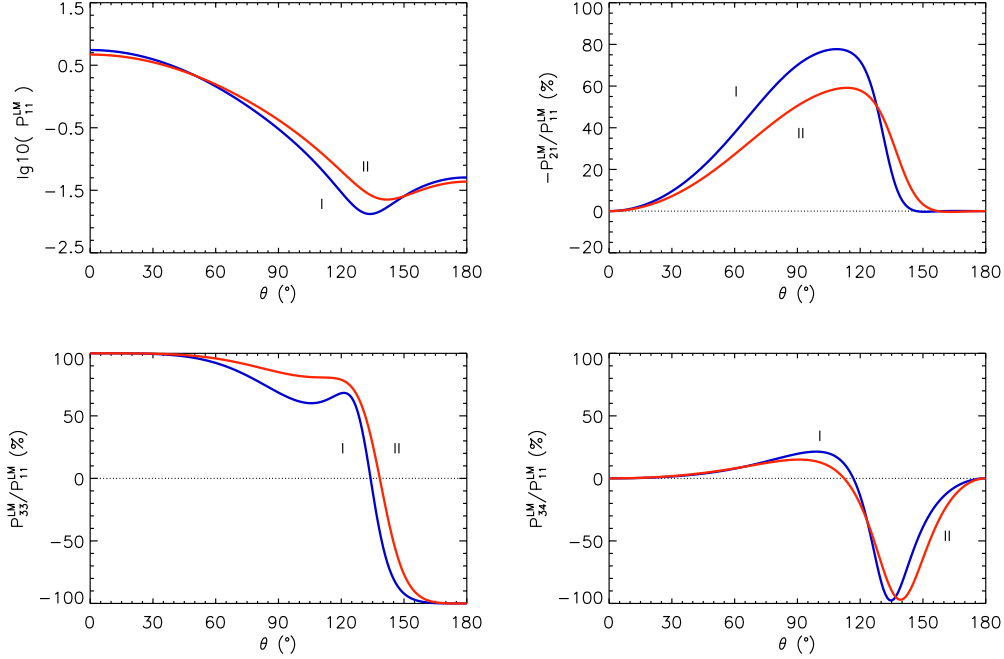
193 and the mean free extinction path length is

$$\ell = \frac{1}{\kappa_{e,\text{ic}}}. \quad (24)$$

194 Finally, the single-scattering albedo of the volume element equals

$$\tilde{\omega}^{\text{ic}} = \frac{\sigma_{s,0}^{\text{ic}}}{\sigma_{e,0}^{\text{ic}}}. \quad (25)$$

195 As for the scattering and absorption characteristics of the discrete random medium,
196 we denote the scattering phase matrix by \mathbf{P} and the spherical albedo equaling the in-
197 coherent single-scattering albedo by A_S .



198 **Figure 2.** Lorenz-Mie scattering matrix elements S_{11}^{LM} (top left), $-S_{21}^{\text{LM}}/S_{11}^{\text{LM}}$ (top right),
 199 $S_{33}^{\text{LM}}/S_{11}^{\text{LM}}$ (bottom left), and $S_{34}^{\text{LM}}/S_{11}^{\text{LM}}$ (bottom right) as a function of the scattering angle
 200 θ for the ice (blue line, Case I) and silicate cases (red line, Case II): Case I, size parameter $x = 2$,
 201 refractive index $m = 1.31$; Case II: $x = 1.76$, $m = 1.50$.

202 3 Numerical methods

203 3.1 Average volume-element characteristics

204 The volume-element scattering, absorption, and extinction characteristics are com-
 205 puted with the help of ensemble-averaging over realizations of randomly distributed spheri-
 206 cal particles in a predefined volume element. We generate the sample volume elements
 207 as follows. First, we draw the number of particles from the Poisson distribution with the
 208 help of the mean number of particles $N_0 = vX_0^3/x^3$ in the volume element. Second, we
 209 place the spherical volume element in the center of a cubic cell that is the unit cell of
 210 a periodically continued random medium of particles. The edgelenhth of the cubic cell
 211 is taken to be large enough (with mean number of particles $> 16N_0$) so that no arti-
 212 ficial disturbances follow for the particle distribution within the spherical volume element.
 213 Third, we generate particles within the cubic cell until the given number of particles are
 214 obtained within the spherical volume element. Fourth, it is clear that the number of par-
 215 ticles in a spherical volume element containing finite-sized particles does not obey the
 216 Poisson distribution. At the final stage, we repeat the aforescribed procedure with a
 217 realistic particle-number variance that we describe later in this section.

218 **Consider next the convergence characteristics of ensemble-averaging for**
 219 **the functions $F(\theta)$ and $G(\theta)$ in Eq. 18. The convergence depends strongly on**
 220 **the scattering angle.** This is due to the phase factor $\exp(i\mathbf{q} \cdot \mathbf{r})$, where $q = |\mathbf{q}| =$
 221 $2k \sin \frac{1}{2}\theta$ varies strongly with the scattering angle. For each scattering angle, we face av-
 222 eraging with a specific apparent wavelength $\lambda/(2 \sin \frac{1}{2}\theta)$. This apparent wavelength ob-
 223 tains the value of $\lambda/2$ in the exact backscattering direction $\theta = 180^\circ$, rising to λ at $\theta =$

224 60°, further to 10λ at $\theta \approx 5.73^\circ$, and reaching infinity in the exact forward scattering
 225 direction.

226 It is thus to be expected that, in the backscattering hemisphere, sufficiently accu-
 227 rate results are obtained for small spherical volume elements from size parameters of roughly
 228 $kR_0 = 10$ upwards. On the contrary, for $\theta = 15^\circ$, even $kR_0 = 40$ does not always suf-
 229 fice. Clearly, a violation of the requirement that the volume-element size must be smaller
 230 than the mean free path length of incoherent extinction can easily result. In the forward
 231 scattering direction, the results nevertheless follow analytically, since the phase factors
 232 reduce to unity.

233 If the incoherent extinction, scattering, and absorption characteristics were inde-
 234 pendent of the volume-element size, we would be able to move forward to the actual RT-
 235 CB computations. There are, however, significant differences in the scattering coefficients
 236 as well as the scattering matrix element S_{11} obtained using different volume elements.
 237 The differences arise from the challenges in the forward-scattering hemisphere described
 238 above.

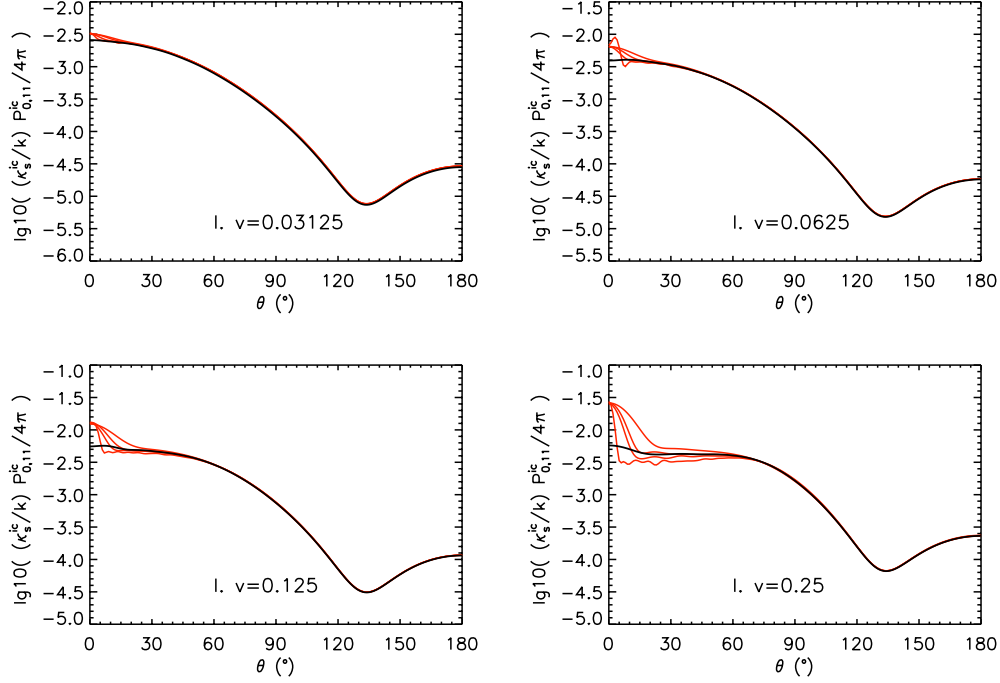
239 In order to obtain unambiguous incoherent input characteristics for the RT-CB code,
 240 we proceed as follows. First, we start by defining the size parameters of the spherical par-
 241 ticle and the spherical volume element x and X_0 , as well as the volume density of par-
 242 ticles v . Second, we generate sample volume elements of spherical particles as described
 243 above. Third, we compute and store the scattered far field and its absolute value squared
 244 from the spherical volume of particles. Here we speed up the convergence with the help
 245 of analytical averaging over orientation for both the scattered far field and its value squared.
 246 Fourth, we repeat the aforescribed steps for a large number of realizations of spheri-
 247 cal volumes of particles. **Fifth, we repeat the entire computation for a number**
 248 **of volume-element size parameters, typically $X_0 = 10, 15, 20$, and 40 .**

249 Finally, we repeat the entire analysis iteratively with a particle-number variance
 250 lowered from the nominal Poisson value until smooth and convergent, maximally invari-
 251 ant incoherent characteristics are obtained for the volume elements near the forward scat-
 252 tering direction. This is a regularization procedure and the true numbers of particles in
 253 the volume elements of an infinite discrete random medium do not necessarily conform
 254 to the statistics imposed here. The procedure allows us to define extinction, scattering,
 255 and absorption characteristics as per volume on a range of sizes slightly above the wave-
 256 length scale. The procedure further underscores how critically important is the actual
 257 number distribution of particles in the volume element.

264 3.2 Radiative-transfer coherent-backscattering method

265 The RT-CB method has been developed originally for homogeneous, finite and semi-
 266 infinite plane-parallel media of spherical scatterers [4]. In what follows, we focus on the
 267 RT-CB computation in a spherical discrete random medium filled with scatterers ([25;
 268 5; 26]). The spherical geometry is attractive due to several reasons. For example, it has
 269 allowed Videen and Muinonen [26] to study light-scattering evolution from single par-
 270 ticles to a regolith by gradually increasing the size of the medium towards macroscopic
 271 scales. For another example, it has allowed detailed comparisons between the RT-CB
 272 method and the STMM method [5].

273 An essential feature of the numerical RT-CB technique is the a priori selection of
 274 scattering directions for updating Stokes parameters during the Monte Carlo radiative-
 275 transfer computation, thus avoiding the collection of rays into finite bins. Fixed angles
 276 allow for the computation of electromagnetic phase differences and thus the coherent-
 277 backscattering effect. In the technique, there are two sets of fixed angles. First, the radiative-
 278 transfer set utilizes Gauss-Legendre abscissae and weights for the phase angle [27] and



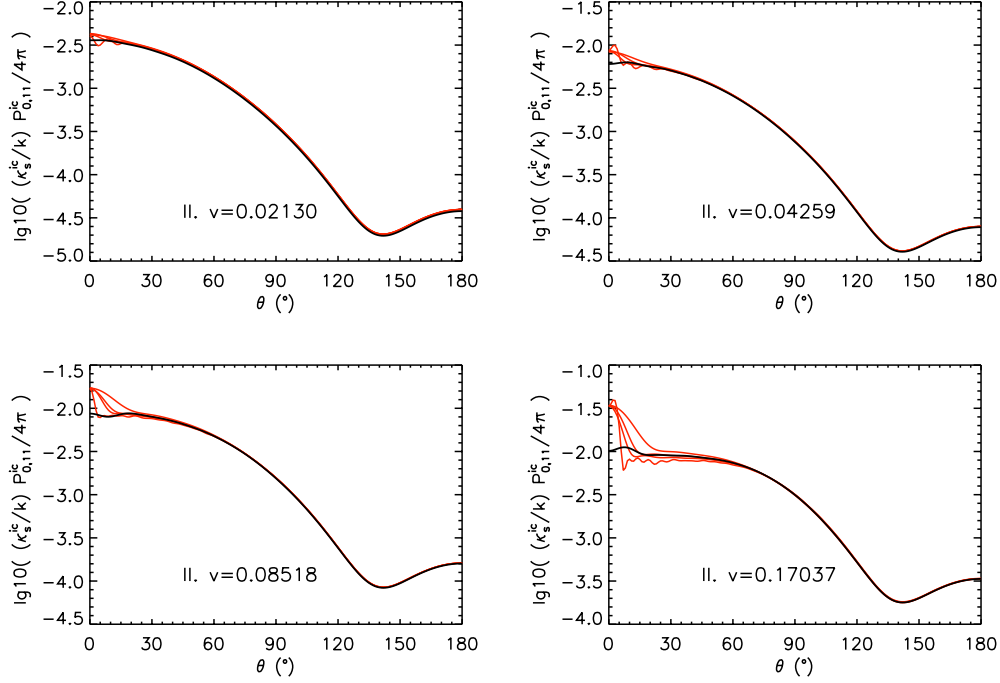
258 **Figure 3.** Volume-element incoherent scattering phase matrix element $P_{0,11}^{ic}$ (scattering phase
 259 function) for Case I (ice) for varying volume elements (thin red lines) as a function of the
 260 scattering angle. The phase function has been normalized to yield the incoherent scattering
 261 coefficient κ_s^{ic}/k upon integration over the solid angle. Also depicted is the final phase function
 262 (thick black line) obtained by regularizing the variance for the number of particles.

279 uniform spacing for the azimuthal angle. Second, the radiative-transfer coherent-backscattering
 280 set can be chosen to cover any angular domain desired.

281 For the RT-CB set, the following angular scheme is incorporated. The azimuthal
 282 angle is uniformly spaced with 8 angles: in general, the number must be a multiple of
 283 8 in order for the azimuthal angle grid to be utilized in the symmetry relations making
 284 the computation efficient. **The phase angle (or backscattering angle)** currently takes
 285 on 51 values between $\alpha = 0.0^\circ$ and $\alpha = 180.0^\circ$ with a concentration of angles near
 286 the backscattering direction.

287 In the generation of new interaction directions, the scattering angle is generated
 288 by using **the cumulative distribution function based on the Mueller element**
 289 $P_{0,11}^{ic}$. Then the Kepler equation is solved using the Newton method for the azimuthal
 290 scattering angle. Within the media, due to constant updating of the Stokes parameters
 291 of scattered light, the generation of directions is coupled with the generation of the path
 292 lengths, confining the subsequent scattering processes into the scattering medium.

293 Since the original numerical method [4], three main changes have been introduced
 294 to make the method more robust and accurate [25; 26]. First, whereas the original method
 295 makes use of the reciprocity relation of electromagnetic scattering in the computation
 296 of the coherent-backscattering contribution in the exact backscattering direction, the present
 297 method utilizes scattering amplitude matrices directly and allows for the reciprocity re-
 298 lation to be used as a measure of computational accuracy.



263

Figure 4. As in Fig. 3 for Case II (silicate).

299

Second, symmetry relations are utilized to improve the numerical convergence of the angular scattering patterns, in particular, in the case of spherical media. There are six incident polarization states that need to be traced in order to obtain the corresponding contributions to the scattering matrix of the spherical medium. In the optimized method, one Markov chain of scatterings is computed in the case of linear polarization and another one in the case of circular polarization. The three remaining linear-polarization chains follow, after proper mapping, from the one computed. Analogously, the one remaining circular-polarization chain follows from the one computed. The improvement of the convergence is substantial and the numerical results have been verified against those from the original method.

309

Third, the finite size of the volume element is accounted for probabilistically. When interaction distances smaller than the volume-element diameter are generated, that is, when the current and the trial next volume-element appear to overlap, we draw a uniform random deviate within $u \in]0, 1[$ and reject the interaction distance if

313

$$u < \frac{\Delta V}{V_0}, \quad (26)$$

314

where ΔV denotes intersectional volume of the two elements. In the case of rejection, we repeat the generation of the distance (together with the direction)

315

4 First results with discussion

316

In what follows, we will compare RT-CB results with those obtained by using the Superposition T -matrix method [2; 1] for a spherical medium (Fig. 1) with **size parameter** $X = kR = 40$ with varying volume density v . For the STMM method, the sample discrete media have been generated using Poisson statistics with the mean number of particles also describing the variance in the number of particles. We point out that,

320

with the RT-CB comparison in mind, what actual distribution one should incorporate for the STMM computations is a nontrivial question.

In terms of composition, we consider two cases of discrete random media composed of equal-sized, non-absorbing spherical particles. In the first case (ice, Case I), the size parameter is $x = 2$ and the refractive index is $m = 1.31$. In the second case (silicate, Case II), the size parameter is $x = 1.76$ and the refractive index is $m = 1.50$. Figure 2 shows the scattering phase matrix elements for the two spherical particles as a function of the scattering angle. These specific kinds of particles have been studied earlier in, e.g., [5], in the context of coherent backscattering by sparse discrete random media. In particular, there is no significant negative polarization in either case (Fig. 2).

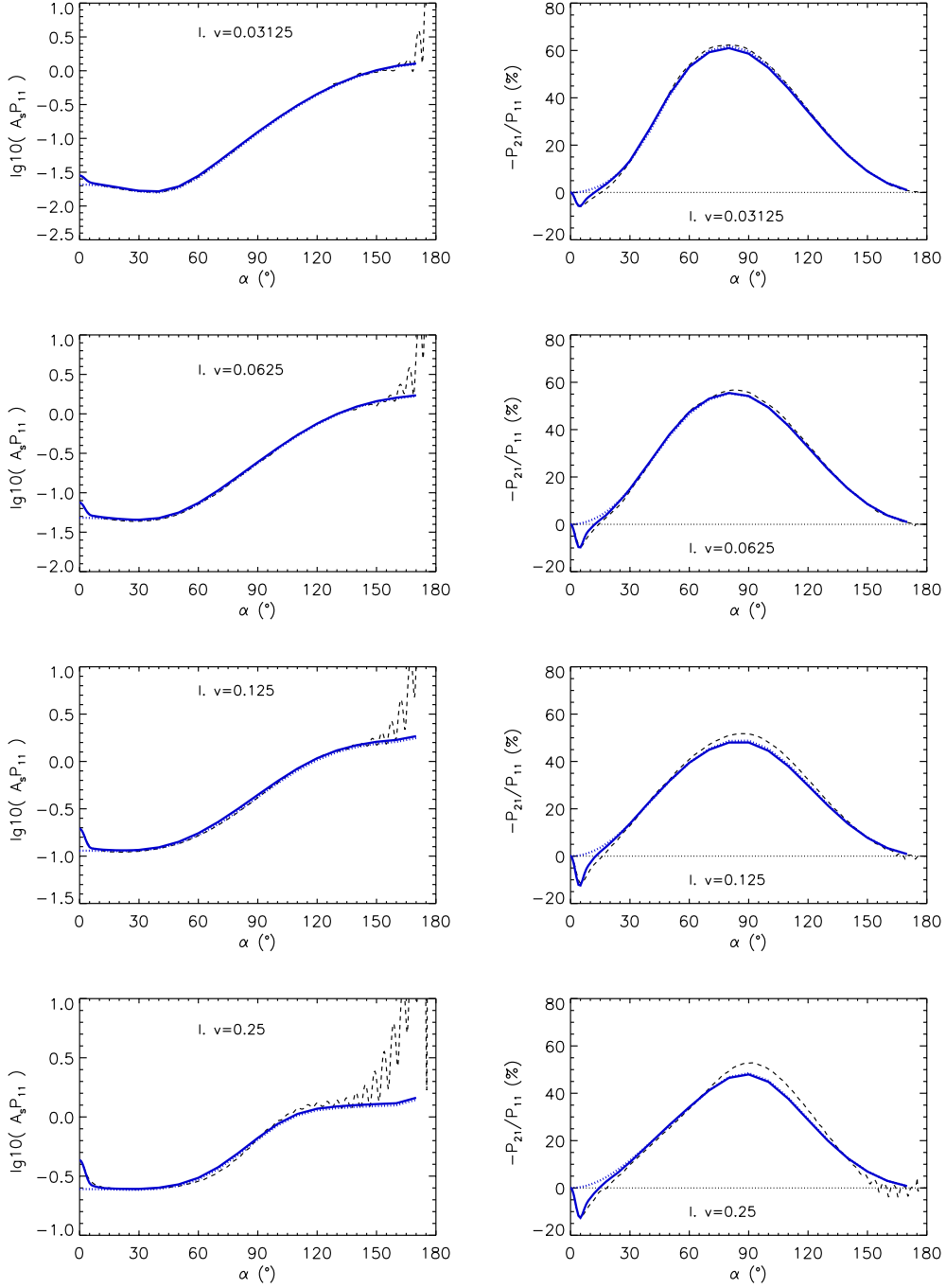
We now compute the incoherent volume-element extinction, scattering, and absorption characteristics. As we consider non-absorbing particles, we are merely concerned with the scattering characteristics, and the incoherent extinction and scattering coefficients coincide. Figures 3 and 4 illustrate the incoherent volume-element scattering phase matrix element $P_{0,11}^{\text{ic}}$ as a function of volume-element size parameter, normalized so as to yield the incoherent scattering coefficient κ_s^{ic}/k upon integration over the full solid angle. Notice that the other matrix elements, expressed as ratios $P_{0,ij}^{\text{ic}}/P_{0,11}^{\text{ic}}$, equal those illustrated in Fig. 2 for the spherical particles.

We have repeated the computation of $(\kappa_s^{\text{ic}}/k)P_{0,11}^{\text{ic}}/(4\pi)$ for **the size parameters** $X_0 = kR_0 = 10, 15, 20,$ and 40 for altogether eight volume densities. For Case I, we assume $v = 3.125\%, 6.25\%, 12.5\%,$ or 25% , corresponding to the mean number of particles of 250, 500, 1000, and 2000, respectively. For Case II, we assume the same mean number of particles, resulting in the volume densities $v = 2.130\%, 4.259\%, 8.518\%,$ or 17.037% . In comparison to our earlier study [5], we have thus added the cases of 1000 and 2000 particles, raising the volume density clearly beyond the validity domain of classical radiative transfer.

Figures 3 and 4 show, first, that the normalized phase functions are in excellent agreement across a wide range of scattering angles from the backscattering hemisphere towards forward scattering. Second, they show the challenges near the forward-scattering direction: a persistent diffraction-like feature appears in all cases. Third, Figures 3 and 4 show that the regularization method relying on downsizing the variance successfully removes the diffraction-like feature. Fourth, for both Cases I and II, the normalized phase function tends to saturate near the forward scattering direction with increasing volume density. Simultaneously, the phase function tends to rise near the backward scattering direction. In conclusion, we can utilize an unambiguous volume-element incoherent scattering phase matrix in RT-CB computations. In detail, we have derived this scattering phase matrix using $X_0 = 15$ and downsizing the variance with the help of the first-round result using $X_0 = 20$ (enforcing the forward-direction value to be equal to the first-round result at $\theta = 10^\circ$).

With the incoherent input parameters in order, we can turn to the RT-CB computation for the discrete spherical random media of spherical particles. Figures 5 and 6 show the results for Cases I and II and certain key numbers are collected in Table 1. For sparse media studied earlier by Muinonen et al. [5] using the RT-CB method with the Lorenz-Mie scattering characteristics as input, the agreement with the STMM results is here even better. We recall that the dense-media RT-CB incorporates a probabilistic treatment for overlapping volume elements, when generating the next interaction point. There is no counterpart in the RT-CB with independent scattering: accounting for the spherical particle size would cause a negligible effect on the angular scattering characteristics.

For the cases of dense media, the RT-CB with incoherent input characteristics works perhaps surprisingly well, considering that only first-order input is utilized. There are



360 **Figure 5.** Scattering phase matrix elements $A_S P_{11}$ and $-P_{21}/P_{11}$ for spherical discrete random
 361 media (size parameter $kR = 40$, varying volume density v) of spherical particles **as a**
 362 **function of the phase angle α .** We show the results for Case I (ice with size parameter $x = 2$
 363 and refractive index $m = 1.31$) as computed using the RT-CB (solid line) and the Superposition
 364 T -matrix methods (dashed line). Also shown **are** the RT-only results (dotted line). A_S denotes
 365 the spherical albedo of the random medium, allowing for absolute comparison between the two
 366 methods.

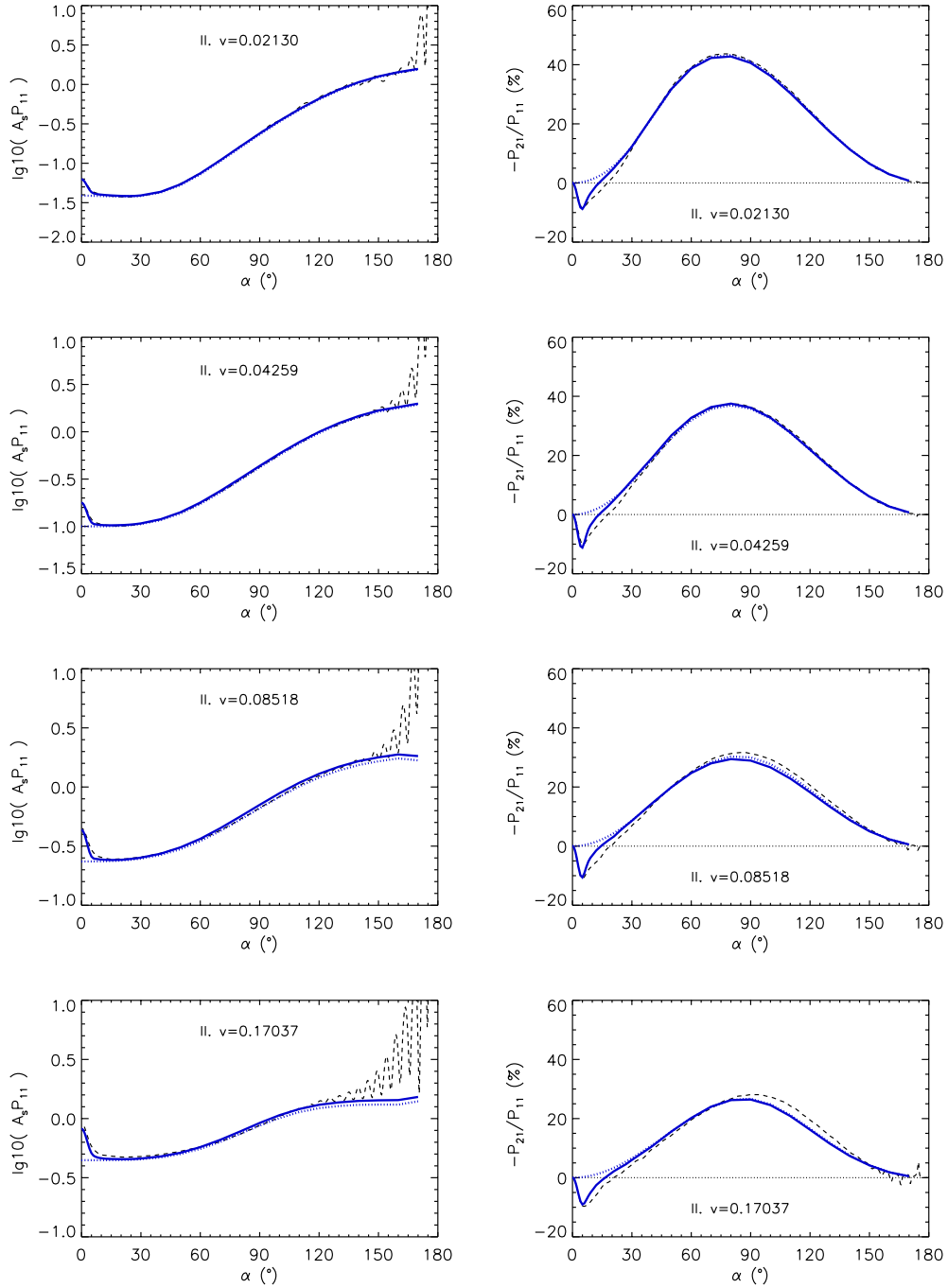


Figure 6. As in Fig. 5 for Case II (silicate) with $x = 1.76$ and $m = 1.50$.

407 **Table 1.** The volume densities v , dimensionless incoherent scattering mean free path lengths
 408 $k\ell$ and coefficients κ_s^{ic}/k , as well as the resulting spherical albedos A_S , geometric albedo p , and
 409 enhancement factors ζ for the cases studied.

Case I, Ice	v	$k\ell$	$\kappa_s^{\text{ic}}/k(10^{-2})$	A_S	$p(\%)$	ζ
	0.03125	155.80	0.64184	0.29	0.68	1.34
	0.06250	83.869	1.1923	0.46	1.79	1.54
	0.12500	50.953	1.9626	0.62	4.89	1.70
	0.25000	39.487	2.5325	0.71	11.16	1.76
Case II, Silicate						
	0.02130	97.726	1.0233	0.41	1.49	1.60
	0.04259	51.181	1.9539	0.62	4.49	1.77
	0.08518	29.540	3.3852	0.79	11.44	1.85
	0.17037	20.128	4.9683	0.88	22.92	1.86

380 deviations between the RT-CB and STMM results in the negative polarization branch,
 381 but these differences may be due to the fact that the discrete medium statistics for gen-
 382 erating the STMM results are bound to differ from the corresponding statistics for the
 383 RT-CB results. The two most important statistical parameters of the discrete random
 384 medium are the mean and variance of the number of particles in the medium.

385 Table 1 shows the evolution of the incoherent extinction mean free path length and
 386 incoherent extinction coefficient for Cases I and II as a function of the volume density.
 387 **It also** shows how the incoherent spherical albedo, geometric albedo, and backscatter-
 388 ing enhancement factor of the discrete random medium evolve with the volume density.
 389 For both cases, the enhancement factor shows saturation towards the highest volume density—
 390 the saturation is stronger for the silicate case where the mean free path lengths are shorter.
 391 **We note that, for $X_0 = 40$, the volume-element size equals the size of the spher-**
 392 **ical random medium itself. Furthermore, for $X_0 = 40$ in Cases I and II as**
 393 **well as for $X_0 = 20$ in Case II, the volume-element size is close to or exceeds**
 394 **the resulting incoherent extinction mean free path length. In spite of the ev-**
 395 **ident violation against the validity criterions (see Sect. 1), we have included**
 396 **these cases in the analysis, too, as they allow for the formal mapping of the**
 397 **mean free path length with increasing volume-element size.**

398 The first results suggest that there is a collective incoherent polarization effect for
 399 phase angles larger than about 90° (**Figs. 5 and 6, bottom right**): there is a tendency
 400 for the exact computation to yield more positive polarization than what results from the
 401 RT-CB computation. This unknown phenomenon can be due to bisphere resonances sim-
 402 ilar to those verified for circular polarization in the backscattering direction by Virkki
 403 et al. [28]. The phenomenon can also be related to the fact that independent orders of
 404 scattering must fail to describe the full scattered field for grazing angles of emergence
 405 (see, e.g., [29; 30]). Studying the ultimate cause for the phenomenon is, however, beyond
 406 the scope of the present study.

410 5 Conclusions

411 We have studied multiple scattering by finite discrete random media of spherical
 412 particles using the radiative-transfer coherent-backscattering method. By introducing
 413 first-order incoherent interaction between the incident field and the volume element, we
 414 have successfully extended the RT-CB method to dense random media markedly beyond
 415 the validity regime of classical radiative transfer.

There are a number of questions arising on the basis of the present study. First, all the current example computations have concerned non-absorbing spherical particles with low to moderately high refractive indices. It remains to be studied where the limits of the first-order incoherent treatment exactly are, a task that can be assessed with the help of the Superposition T -matrix method. Second, it is our near-term plan to replace the first-order incoherent interaction with a rigorous treatment, again, using T -matrices. Finally, third, we intend to incorporate nonspherical particles and extend the numerical methods accordingly.

Acknowledgments

The research has been supported by the European Research Council with Advanced Grant No. 320773 SAEMPL, Scattering and Absorption of ElectroMagnetic waves in Particle-Late media. The computational resources have been provided by CSC — IT Centre for Science Ltd, Finland.

References

- [1] Mackowski, D. W., and Mishchenko, M. I. (2011). A multiple sphere T-matrix FORTRAN code for use on parallel computer clusters. *J. Quant. Spectrosc. Radiat. Transfer* 112, 2182–2192.
- [2] Markkanen, J., and Yuffa, A. J. (2017). Fast superposition T-matrix solution for clusters with arbitrarily-shaped constituent particles. *J. Quant. Spectrosc. Radiat. Transfer* 189, 181–189.
- [3] Ylä-Oijala, P., Markkanen, J., Järvenpää, S., and Kiminki, S. P. (2014). Surface and Volume Integral Equation Methods for Time-Harmonic Solutions of Maxwell’s Equations. *Progress Electromagnetics Res.* 149, 15–44.
- [4] Muinonen, K. (2004). Coherent backscattering of light by complex random media of spherical scatterers: numerical solution. *Waves Random Media* 14, 365–388.
- [5] Muinonen, K., Mishchenko, M. I., Dlugach, J. M., Zubko, E., Penttilä, A., and Videen, G. (2012). Coherent backscattering verified numerically for a finite volume of spherical particles. *Astrophys. J.*, 760, 118, 11 pp.
- [6] Barabashev, N. P. (1922). Bestimmung der Erdalbedo und des Reflexionsgesetzes für die Oberfläche der Mondmeere. Theorie den Rillen. *Astron. Nachr.* 217, 445–452.
- [7] Lyot, B. (1929). Recherches sur la polarisation de la lumière des planètes et de quelques substances terrestres *Ann. Obs. Paris* 8(1), 1–161.
- [8] Shkuratov, Y. G. (1985). *Astronomicheskii Tsirkular* 1400, 3 (Shternberg State Astron. Institute, Moscow).
- [9] Muinonen, K. (1989). Electromagnetic scattering by two interacting dipoles. In *URSI Electromagnetic Theory Symposium (EMTS’89)*, 428–430.
- [10] Muinonen, K., Markkanen, J., Penttilä, A., Väisänen, T., and Peltoniemi, J. (2016). Multiple scattering by dense random media: Numerical solution. In *Electromagnetic Theory Symposium (EMTS’16)*, 400–403.
- [11] Muinonen, K., Markkanen, J., Penttilä, A., Virkki, A., and Mackowski, D. (2016). Multiple scattering by dense random media: Incoherent extinction. In *URSI Electromagnetic Theory Symposium (EMTS’16)*, 751–754 (2016).
- [12] Zurk, L. M., Tsang, L., Ding, K. H., and Winebrenner, D. P. (1995). Monte Carlo simulations of the extinction rate of densely packed spheres with clustered and nonclustered geometries, *J. Opt. Soc. Am. A* 12, 1772–1781.
- [13] Lu, C. C., Chew, W. C., and Tsang, L. (1995). The application of recursive aggregate T-matrix algorithm in the Monte Carlo simulations of the extinction rate of random distribution of particles, *Radio Sci.* 30(1), 25–28.

- 466 [14] Tsang, L., Kong, J. A., Shin, R. T. (1985). *Theory of Microwave*
 467 *Remote Sensing*, New York, Wiley.
- 468 [15] Tsang, L., and Ishimaru, A. (1987). Radiative wave equations for vector electro-
 469 magnetic propagation in dense nontenuous media. *J. Electromagn. Waves Appl.*
 470 1(1), 59–72.
- 471 [16] Mishchenko, M. I., Travis, L. D., and Lacis, A. A. (2006). *Multiple Scattering of*
 472 *Light by Particles*, Cambridge, United Kingdom: Cambridge University Press.
- 473 [17] Bohren, C. F., and Huffman, D. R. (1983). *Absorption and Scattering of Light*
 474 *by Small Particles*, New York, Wiley.
- 475 [18] Cruzan, O. R. (1962). Translation addition theorems for spherical vector wave
 476 function'. *Quart. Appl. Math.* 20, 33–40.
- 477 [19] Greengard, L., and Rokhlin, V. (1987). A fast algorithm for particle simula-
 478 tions. *J. Comp. Physics* 73, 325–348.
- 479 [20] Gumerov, N. A., and Duraiswami, R. (2005). Computation of scattering from
 480 clusters of spheres using the fast multipole method. *J. Acoust. Soc. America* 117,
 481 1744–1761.
- 482 [21] Chew, W. C. (1992). Recurrence relations for three-dimensional scalar addition
 483 theorem. *J. Electromagn. Waves Applic.* 6, 133–142.
- 484 [22] Choi, C. H., Ivanic, J., Gordon, M. S., and Ruedenberg, K. (1999). Rapid and
 485 stable determination of rotation matrices between spherical harmonics by direct
 486 recursion. *J. Chem. Physics* 111, 8825–8831.
- 487 [23] Debye, P. (1915). Zerstreuung von Röntgenstrahlen. *Ann. Phys.* 46, 809–823.
- 488 [24] Muinonen, K. (1996). Light scattering by Gaussian random particles: Rayleigh
 489 and Rayleigh–Gans approximations. *J. Quantitat. Spectrosc. Radiat. Transfer* 55,
 490 603–613.
- 491 [25] Muinonen, K., and Videen, G. (2012). A phenomenological single scatterer for
 492 studies of complex particulate media. *J. Quant. Spectrosc. Radiat. Transfer* 113,
 493 2385–2390.
- 494 [26] Videen, G., and Muinonen, K. (2015). Light-scattering evolution from particles
 495 to regolith. *J. Quant. Spectrosc. Radiat. Transfer* 150, 87–94.
- 496 [27] Press, W. H., Teukolsky, S. A., Vetterling, W. T., and Flannery, B. P. (1992).
 497 *Numerical Recipes in Fortran, The Art of Scientific Computing*, Second Edition,
 498 Cambridge University Press.
- 499 [28] Virkki, A., Markkanen, J., Tyynelä, J., Peltoniemi, J. I., and Muinonen, K.
 500 (2015). Polarization by clusters of spherical particles at backscattering. *Optics*
 501 *Letters* 40(15), 3663–3666.
- 502 [29] Lindell, I. V., Sihvola, A. H., Muinonen, K. O., and Barber, P. W. (1991). Scat-
 503 tering by a small object close to an interface. I: Exact Image Theory formulation.
 504 *J. Opt. Soc. America A* 8, 472–476.
- 505 [30] Muinonen, K. O., Sihvola, A. H., Lindell, I. V., and Lumme, K. A. (1991).
 506 Scattering by a small object close to an interface. II: Study of backscattering. *J.*
 507 *Opt. Soc. America A* 8, 477–482.